Journal of Medicinal Chemistry

Article

Substituted 2-acylamino-cycloalkylthiophene-3-carboxylic acid arylamides as inhibitors of the calcium-activated chloride channel transmembrane protein 16A (TMEM16A)

Eric C Truong, Puay-Wah Phuan, Amanda L Reggi, Loretta Ferrera, Luis J.V. Galietta, Sarah E Levy, Alannah C Moises, Onur Cil, Elena Diez-Cecilia, Sujin Lee, Alan S Verkman, and Marc O. Anderson

J. Med. Chem., **Just Accepted Manuscript** • Publication Date (Web): 11 May 2017

Substituted 2-acylamino-cycloalkylthiophene-3-carboxylic acid arylamides as inhibitors of the calcium-activated chloride channel transmembrane protein 16A (TMEM16A)

Eric C. Truong[1], Puay W. Phuan[2], Amanda L. Reggi[1], Loretta Ferrera[3], Luis J.V. Galietta[4], Sarah E. Levy[1], Alannah C. Moises[1], Onur Cil[2], Elena Diez-Cecilia[1], Sujin Lee[2], Alan S. Verkman[2], and Marc O. Anderson[1*]

[1]Department of Chemistry and Biochemistry, San Francisco State University, San Francisco CA, 94132-4136 USA; [2]Departments of Medicine and Physiology, University of California, San Francisco CA, 94143-0521 USA; [3]U.O.C. Genetica Medica, Istituto Giannina Gaslini, Genova, ITALY; [4]Telethon Institute of Genetics and Medicine (TIGEM), Pozzuoli (NA), ITALY.

Corresponding author: Marc O. Anderson, Ph.D. Department of Chemistry and Biochemistry, San Francisco State University, San Francisco CA 94132. Phone 415-338-6495; Fax 415-405-0377; email marc@sfsu.edu.

Keywords: TMEM16A, calcium-activated chloride channel, ANO1, hypertension, cancer, anoctamin, cycloalkylthiophene, 2-acylamino-cycloalkylthiophene-3-carboxylic acid arylamide

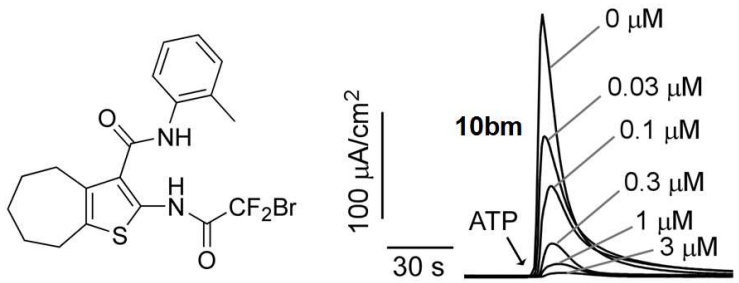

10bm IC_{50} = 30 nM TMEM16A short-circuit current

ABSTRACT

Transmembrane protein 16A (TMEM16A), also called anoctamin 1 (ANO1), is a calcium-activated chloride channel expressed widely mammalian cells, including epithelia, vascular smooth muscle tissue, electrically excitable cells and some tumors. TMEM16A inhibitors have been proposed for treatment of disorders of epithelial fluid and mucus secretion, hypertension, asthma, and possibly cancer. Herein we report by screening the discovery of 2-acylamino-cycloalkylthiophene-3-carboxylic acid arylamides (AACTs) as inhibitors of TMEM16A, and analysis of 48 synthesized analogs (**10ab-10bw**) of the original AACT compound (**10aa**). Structure-activity studies indicated the importance of benzene substituted as 2- or 4-methyl, or 4-fluoro, and defined the significance of thiophene substituents and size of the cycloalkylthiophene core. The most potent compound (**10bm**), which contains an unusual bromodifluoroacetamide at the thiophene 2-position, had IC_{50} ~ 30 nM, ~3.6-fold more potent than the most potent previously reported TMEM16A inhibitor **4** (Ani9), and >10-fold metabolic stability. Direct and reversible inhibition of TMEM16A by **10bm** was demonstrated by patch-clamp analysis. AACTs may be useful as pharmacological tools to study TMEM16A function and as potential drug development candidates.

INTRODUCTION

Transmembrane protein 16A (also known as TMEM16A, ANO1, DOG1, ORAOV2, TAOS-2) is a calcium-activated chloride channel (CaCC) that is expressed in a variety of mammalian tissues including smooth muscle cells, airway mucin-secreting cells, secretory epithelia, interstitial cells of Cajal, and nociceptive neurons.[1-3] TMEM16A is overexpressed in some human cancers,[4, 5] and knockdown of TMEM16A inhibits cancer cell proliferation, cell cycle progression, and apoptosis.[6] TMEM16A was reported recently as a biomarker for gastrointestinal stromal and esophageal tumors,[7, 8] and TMEM16A expression is associated with good prognosis in PR-positive or HER2-negative breast cancer following tamoxifen treatment.[9]

Early studies suggested TMEM16A contains eight putative transmembrane domains with intracellular N- and C- termini, and two calmodulin binding domains.[10-12] Multiple TMEM16A splice variants may explain its variable behavior in different tissues and cell types.[13-16] Recent studies have questioned the role of calmodulin in TMEM16A activation, and have identified four acidic side-chain residues involved in Ca^{2+} binding in mouse TMEM16A: E698, E701, E730 and D734.[17, 18] Other divalent cations (Sr^{2+} and Ni^{2+}) appear to activate the channel as well.[19] Four basic side-chain residues appear to be critical for anion selectivity in mouse TMEM16A: R511, K599, R617 and R784.[20] The kinetics of TMEM16A and TMEM16B Cl^- conductance are complex, with distinct fast and slow gating mechanisms, regulated by membrane voltage and Cl^- concentration.[21] Biophysical experiments suggest TMEM16A is present in membranes as a homodimer,[22, 23] with the dimerization domain located in the N-terminal sequence.[24] Recently, the C-terminal region of TMEM16A was modified to produce a constitutively active channel, providing a strategy to design TMEM16A activators.[25]

A 3.4Å X-ray crystal structure was solved recently of a Ca^{2+}-activated lipid scramblase expressed in the fungus *Nectria haematococca* (nhTMEM16), which is ~ 40% homologous to mammalian TMEM16A, indicating a ten-transmembrane helical structure.[26] Using the nhTMEM16 structure, two

homology models of TMEM16A suggest it contains ten transmembrane helical segments,[21, 25] revising earlier eight helix structural models.

Inhibitors of TMEM16A has been proposed to be of potential utility for treatment of hypertension, asthma, inflammatory and reactive airways diseases, pain, and possibly cancer.[1, 3, 4, 27] Reported inhibitors (Figure 1) include the non-selective CaCC inhibitor $CaCC_{inh}$-A01 (**1**),[28] and TMEM16A-selective inhibitors such as the thiopyrimidine aryl aminothiazole $T16A_{inh}$-A01 (**2**),[29, 30] N-((4-methoxy)-2-naphthyl)-5-nitroanthranilic acid (MONNA) (**3**),[31] and the acyl hydrazone Ani9 (**4**).[32] The use of compound **2** to inhibit TMEM16A in various tissues has been reviewed.[1] Compound **2** blocks Ca^{2+}-activated Cl^- currents in vascular smooth muscle cells, and relaxes mouse and human blood vessels,[33] This compound also prevents serotonin-induced contractile responses in pulmonary arteries of chronic hypoxic rats, a model of pulmonary hypertension,[34] and reverses EGF-induced increases in CaCC currents in T84 colonic epithelial cells.[35] Recently, **2** was also shown to attenuate angiotensin II-induced cerebral vasoconstriction in rat basilar arteries, further supporting TMEM16A as a target in vascular function, hypertension, and stroke.[36] The non-selective CaCC inhibitor **1** was shown to accelerate the degradation of TMEM16A in cancer cells by the ubiquitin-proteasome pathway by a mechanism that may not involve channel inhibition.[37] Several recent studies address inhibitor selectivity. Studies of **1**, **2**, and **3** in isolated resistance arteries suggested poor TMEM16A selectivity for all three compounds.[38] Another study reported **1** as a non-selective inhibitor of CaCCs TMEM16A and Bestrophin1, while **2** selectively inhibited TMEM16A but with low potency.[39] As such, the discovery of potent and selective TMEM16A inhibitors continues to be a focus of multiple laboratories.

Herein, we report the discovery by screening of a 2-acylamino-cycloalkylthiophene-3-carboxylic acid arylamide (AACT) class of TMEM16A inhibitors, exemplified by **10aa**. Synthesis and evaluation of 48 analogs of **10aa** has provided compounds with substantially improved TMEM16A inhibition potency and metabolic stability than the recently reported compound **4**.

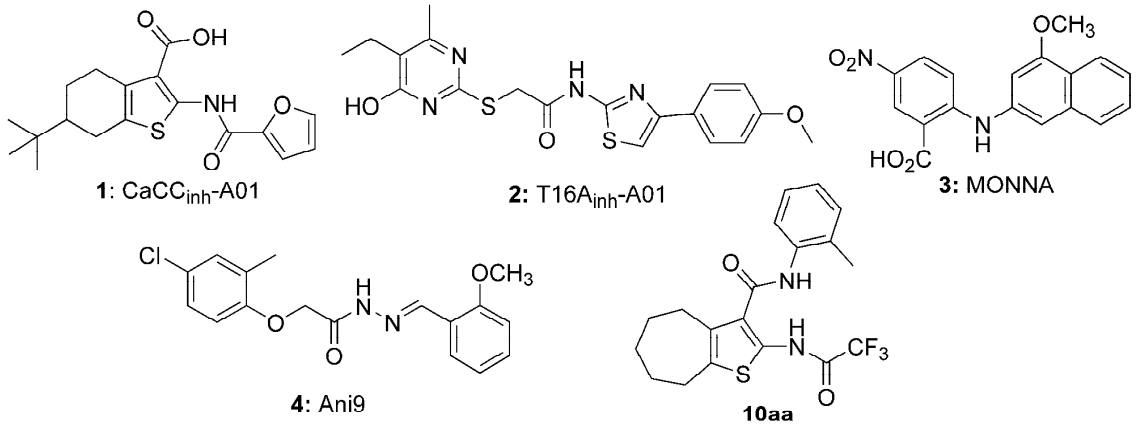

Figure 1. Structures of the non-selective CaCC inhibitor **1**,[28] and TMEM16A inhibitors **2**,[29, 30] **3**,[31] **4**,[32] and the new class of cycloalkylthiophene inhibitors (**10aa**) described herein.

RESULTS AND DISCUSSION

A medium-throughput screening assay was previously developed to identify small molecule inhibitors of TMEM16A.[40] The screen utilized FRT cells that were stably transfected with human TMEM16A and the iodide-sensitive fluorescent protein YFP-H148Q/I152L/F46L. The assay involved addition of test compounds to the cells for 10 min in a physiological chloride-containing solution, followed by addition of an iodide solution containing ATP. ATP is a P2Y2 agonist in FRT cells used to increase cytosolic Ca^{2+} and activate TMEM16A channels. TMEM16A-facilitated iodide influx was determined from the initial time course of decreasing YFP fluorescence. TMEM16A inhibitors reduce iodide influx, resulting in a reduced rate of decreasing fluorescence. Here, screening of 50,000 drug-like synthetic small molecules not previously tested identified 2-acylamino-cycloalkylthiophene-3-carboxylic acid arylamide (AACT) **10aa** with IC_{50} ~ 0.42 μM (Figure 2). The structure of **10aa** resembles that of the previously identified non-selective CaCC inhibitor **1**,[28] although the latter molecule is substituted with a *tert*-butyl group, has a different assortment of functionality on the thiophene (e.g. lacking the haloacetamide), and was reported to be significantly less potent (IC_{50} = 2.1 μM) than **10aa** against TMEM16A.[29]

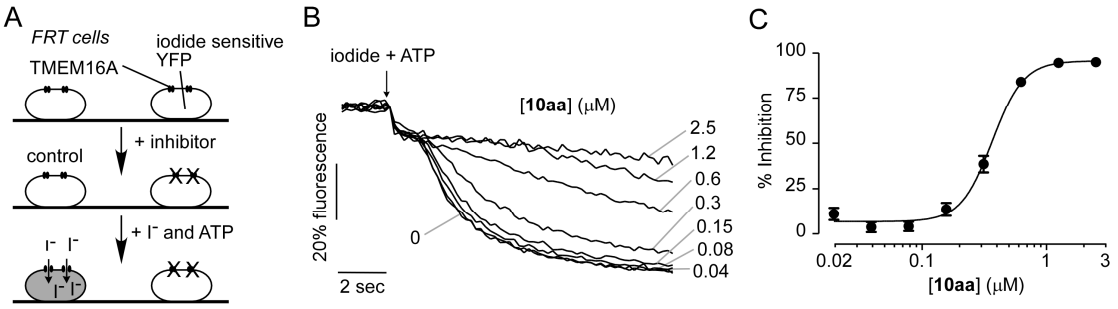

Figure 2. Identification of TMEM16A inhibitors. A. Schematic of assay. FRT cells stably expressing TMEM16A and a halide-sensitive YFP sensor were incubated for 10 min with test compound. Extracellular addition of addition of iodide and ATP results in YFP quenching whose rate is reduced by TMEM16A inhibition. B. Original fluorescence quenching curves for inhibition of TMEM16A by **10aa**. C. Concentration-dependent inhibition of TMEM16A by **10aa** (mean ± S.E., n=4).

Motivated by the submicromolar potency of **10aa** and the modularity and synthetic accessibility of this scaffold, we further optimized this class of compounds. The only other reported biological activity of AACT compounds is inhibition of the protozoan parasite *Leishmania donovani* (EC_{50} = 6.4 μM), with no cytotoxicity seen against human macrophages (CC_{50} > 50 μM).[41] The most potent inhibitor in the anti-parasite study was an analog of **10aa**, with 2-methylanilide replaced with 4-methoxyanilide.

Chemistry

AACT compounds were prepared using the modular synthetic strategy shown in Scheme 1. The synthesis begins with the generation of substituted aryl cyanoacetamides, followed by a two-step Knoevenagel-Gewald sequence to generate 2-aminothiophenes, and coupling with simple electrophilic acylating agents. Substituted anilines (**5a-5k**) were coupled with cyanoacetic acid using EDCI-HCl to generate the library of cyanoacetamides (**6a-6k**). The substituent composition of this

library, prepared typically in good yields, is reported in Table 1, with some of the cyanoacetamides also being commercially available.

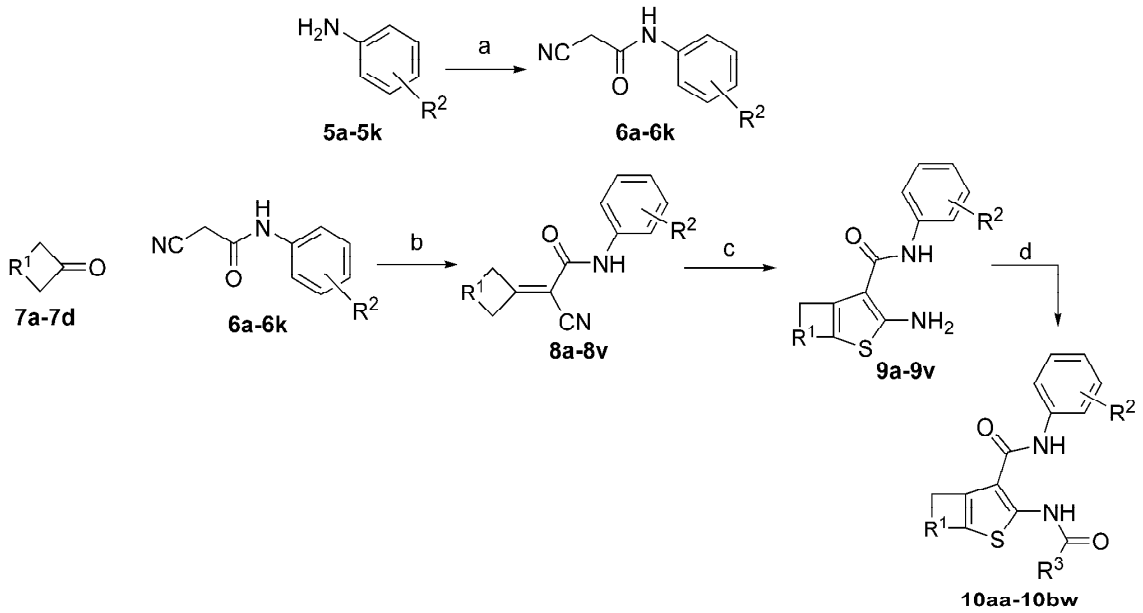

Scheme 1. Synthesis of 2-acylamino-cycloalkylthiophene-3-carboxylic acid arylamides. *Reagents and conditions*: (a) cyanoacetic acid (1.0 eq) and EDCI-HCl (1.2 eq) (rt, 6 min); (b) cycloalkyl ketone, NH_4OAc, and AcOH (100 ^oC, 60 min); (c) S_8, morpholine (3.0 eq), EtOH (90 ^0C, 5h); (d) electrophilic acylating agent (1.3 eq), Et_3N (1.3 eq) (rt, 10 min) or difluoroiodoacetic acid (1.2 eq) and EDCI-HCl (1.5 eq) (rt, 60 min).

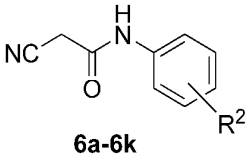

Table 1. Synthesis yields for EDCI-mediated cyanoacetamide generation reactions (**5 → 6**); yields (%) are of the isolated or purified products. Purity of compounds was >95% based on HPLC-LCMS analysis at 254 nm, and absence of impurities was confirmed by ^1H NMR spectra.

Product Cyano-acetamide	SM Aniline	R^2	Isolated Yield (%)
6a	**5a**	2-(CH_3)	50
6b	**5b**	H	purchased
6c	**5c**	2-(CH_2CH_3)	76
6d	**5d**	2-F	78
6e	**5e**	4-F	70
6f	**5f**	2-Cl	82
6g	**5g**	3-Cl	80
6h	**5h**	4-Cl	89
6i	**5i**	4-(CF_3)	79
6j	**5j**	4-(CH_3)	86
6k	**5k**	2-(OCF_3)	87

Next, the substituted aryl cyanoacetamides (**6a-6k**) were condensed with a small collection of cycloalkyl ketones (**7a-7d**) under buffered acid-catalyzed aldol conditions (AcOH:NH_4OAc) to generate Knoevenagel adducts (**8a-8v**). While excess cyclic ketone was useful to obtain high conversion, we were pleased that this material could be removed by evaporation. The Knoevenagel adducts were subjected to the Gewald cyclization reaction in the presence of molecular octasulfur (S_8), to yield 2-amino-cycloalkylthiophene-3-carboxylic acid arylamides (**9a-9v**), which were typically crystalline and easily purified by trituration. The composition of the library and yields for the Knoevenagel and Gewald reactions are reported in Table 2, separated by the different cycloalkyl ketones.

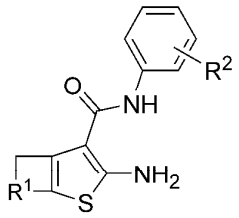

9a-9v

Table 2. Synthesis yields for Knoevenagel reaction / aminothiophene formation (**7** + **6** → [**8**] → **9**). Yields (%) are of the isolated or purified products. Purity of compounds was >95% based on HPLC-LCMS analysis at 254 nm, and absence of impurities was confirmed by ^{1}H NMR spectra.

Product Amino-thiophene	SM Cyano-acetamide	Isolated Yield (%) Intmdt 8a-8v	Isolated Yield (%) Product 9a-9v	R^1	R^2
*(based on cycloheptanone **7a**)*					
9a	**6a**	87	50	$-(CH_2)_4-$	2-(CH_3)
9b	**6b**	52	90	$-(CH_2)_4-$	H
9c	**6c**	48	70	$-(CH_2)_4-$	2-(CH_2CH_3)
9d	**6d**	93	51	$-(CH_2)_4-$	2-F
9e	**6e**	60	69	$-(CH_2)_4-$	4-F
9f	**6f**	70	85	$-(CH_2)_4-$	2-Cl
9g	**6g**	73	93	$-(CH_2)_4-$	3-Cl
9h	**6h**	90	67	$-(CH_2)_4-$	4-Cl
9i	**6i**	76	98	$-(CH_2)_4-$	4-(CF_3)
9j	**6j**	58	7	$-(CH_2)_4-$	2-(OCF_3)
*(based on cyclohexanone **7b**)*					
9k	**6b**	70	62	$-(CH_2)_3-$	H
9l	**6a**	90	95	$-(CH_2)_3-$	2-(CH_3)

9m	**6j**	55	37	$-(CH_2)_3-$	4-(CH_3)
9n	**6e**	32	97	$-(CH_2)_3-$	4-F
*(based on tetrahydro-4H-pyran-4-one **7c**)*					
9o	**6a**	86	92	$-CH_2OCH_2-$	2-(CH_3)
9p	**6f**	66	21	$-CH_2OCH_2-$	2-Cl
9q	**6j**	55	23	$-CH_2OCH_2-$	4-(CH_3)
9r	**6e**	70	26	$-CH_2OCH_2-$	4-F
*(based on cyclopentanone **7d**)*					
9s	**6a**	60	92	$-(CH_2)_2-$	2-(CH_3)
9t	**6j**	60	55	$-(CH_2)_2-$	4-(CH_3)
9u	**6f**	84	72	$-(CH_2)_2-$	2-Cl
9v	**6k**	38	82	$-(CH_2)_2-$	2-(OCF_3)

Finally, coupling of the aminothiophenes (**9a-9v**) with alkyl and fluoroalkyl acyl chlorides, anhydrides, or EDCI-coupling was done to generate the final desired AACT compounds (**10aa-10bw**), also typically as crystalline solids, in fair to good yields (Table 3). After completion of a 1st generation of compounds (**10aa-10bj**) based on simple alkyl and fluoroalkyl groups at the R^3 position, we designed a 2nd generation library with halodifluoroalkyl (chloro, bromo, and iodo) and heptafluorobutyryl at R^3, based on the most promising combinations of R^1 and R^2 (**10bk-10bw**). The synthesis of the difluoroiodoacetyl inhibitors (**10bn**, **10bq**, **10bt**, and **10bw**) was accomplished by EDCI-mediated coupling of aminothiophenes with difluoroiodoacetic acid. In total, 49 inhibitor candidates were prepared by variations at the R^1, R^2, and R^3 positions. The structure and purity of the final products were confirmed by ^{1}H-NMR, ESI-LCMS (UV absorption detection at 254 nm), with purities estimated to be >95%.

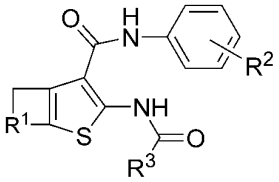

10aa-10bw

Table 3. Coupling yields and TMEM16A inhibition of AACT compounds (**10aa-10bw**). Yields (%) are of the isolated or purified products. IC_{50} (μM) for inhibition of TMEM16A anion conductance using a fluorescence plate reader (FPR) assay (SEM in parentheses; n = 3). Purity of assayed compounds was >95% based on HPLC-LCMS analysis at 254 nm, and absence of impurities was confirmed by inspection of ^{1}H NMR spectra. [a]Low solubility in DMSO.

Product Final	SM Amino thiophene	R^1	R^2	R^3	Isolated Yield (%)	FPR IC_{50} TMEM16A (μM)
*(based on cycloheptanone **7a**)*						
10aa	**9a**	$-(CH_2)_4-$	2-(CH_3)	CF_3	61	0.42 (0.03)
10ab	**9a**	$-(CH_2)_4-$	2-(CH_3)	CF_2CF_3	65	1.3
10ac	**9a**	$-(CH_2)_4-$	2-(CH_3)	CH_3	82	>10
10ad	**9a**	$-(CH_2)_4-$	2-(CH_3)	CH_2CH_3	70	>20
10ae	**9b**	$-(CH_2)_4-$	H	CF_3	38	0.3 (0.005)
10af	**9b**	$-(CH_2)_4-$	H	CF_2CF_3	97	2.5
10ag	**9b**	$-(CH_2)_4-$	H	CH_3	80	>20
10ah	**9b**	$-(CH_2)_4-$	H	CH_2CH_3	87	1.2
10ai	**9c**	$-(CH_2)_4-$	2-(CH_2CH_3)	CF_3	6	1.3 (0.7)
10aj	**9d**	$-(CH_2)_4-$	2-F	CF_3	48	1.3
10ak	**9e**	$-(CH_2)_4-$	4-F	CF_3	60	0.32 (0.11)
10al	**9f**	$-(CH_2)_4-$	2-Cl	CF_3	87	0.66 (0.02)
10am	**9f**	$-(CH_2)_4-$	2-Cl	CF_2CF_3	91	>20

10an	**9g**	$-(CH_2)_4-$	3-Cl	CF_3	23	5 (0.2)
10ao	**9h**	$-(CH_2)_4-$	4-Cl	CF_3	4	3 (0.09)
10ap	**9i**	$-(CH_2)_4-$	4-(CF_3)	CF_3	2	5 (0.10)
10aq	**9j**	$-(CH_2)_4-$	2-(OCF_3)	CF_3	12	1.3 (0.2)
10ar	**9j**	$-(CH_2)_4-$	2-(OCF_3)	CF_2CF_3	30	2.7 (0.07)
10as	**9j**	$-(CH_2)_4-$	2-(OCF_3)	CH_3	55	>20
10at	**9j**	$-(CH_2)_4-$	2-(OCF_3)	CH_2CH_3	50	>20
*(based on cyclohexanone **7b**)*						
10au	**9k**	$-(CH_2)_3-$	H	CF_3	93	0.37 (0.01)
10av	**9l**	$-(CH_2)_3-$	2-(CH_3)	CF_3	17	0.17 (0.001)
10aw	**9m**	$-(CH_2)_3-$	4-(CH_3)	CF_3	30	0.22 (0.01)
10ax	**9n**	$-(CH_2)_3-$	4-F	CF_3	48	0.49 (0.02)
*(based on tetrahydro-4H-pyran-4-one **7c**)*						
10ay	**9o**	$-CH_2OCH_2-$	2-(CH_3)	CF_2CF_3	6	1.6 (0.09)
10az	**9o**	$-CH_2OCH_2-$	2-(CH_3)	CH_2CH_3	40	3 (0.09)
10ba	**9p**	$-CH_2OCH_2-$	2-Cl	CF_3	67	1.3
10bb	**9q**	$-CH_2OCH_2-$	4-(CH_3)	CF_3	38	5 (0.1)
10bc	**9r**	$-CH_2OCH_2-$	4-F	CF_3	15	3.8 (0.09)
*(based on cyclopentanone **7d**)*						
10bd	**9s**	$-(CH_2)_2-$	2-(CH_3)	CF_3	10	>20
10be	**9s**	$-(CH_2)_2-$	2-(CH_3)	CF_2CF_3	37	6.2
10bf	**9s**	$-(CH_2)_2-$	2-(CH_3)	CH_3	38	>20
10bg	**9s**	$-(CH_2)_2-$	2-(CH_3)	CH_2CH_3	33	>20
10bh	**9t**	$-(CH_2)_2-$	4-(CH_3)	CF_3	77	2.5 (0.04)
10bi	**9u**	$-(CH_2)_2-$	2-Cl	CF_3	64	1.3
10bj	**9v**	$-(CH_2)_2-$	2-(OCF_3)	CF_3	56	0.37 (0.02)
(2nd-generation inhibitors with novel R^3 substituents, including chloro/bromo/iodo difluoroacetyl)						
10bk	**9a**	$-(CH_2)_4-$	2-(CH_3)	CF_2Cl	27	0.18 (0.008)

10bl	**9a**	$-(CH_2)_4-$	2-(CH_3)	$CF_2CF_2CF_3$	61	0.38 (0.01)
10bm	**9a**	$-(CH_2)_4-$	2-(CH_3)	CF_2Br	36	0.083 (0.007)
10bn	**9a**	$-(CH_2)_4-$	2-(CH_3)	CF_2I	67	0.6 (0.02)
10bo	**9b**	$-(CH_2)_4-$	H	CF_2Cl	16	0.925 (0.002)
10bp	**9b**	$-(CH_2)_4-$	H	CF_2Br	15	0.23 (0.004)
10bq	**9b**	$-(CH_2)_4-$	H	CF_2I	13	0.23 (0.004)
10br	**9e**	$-(CH_2)_4-$	4-F	CF_2Cl	19	0.84 (0.04)
10bs	**9e**	$-(CH_2)_4-$	4-F	CF_2Br	32	0.45 (0.03)
10bt	**9e**	$-(CH_2)_4-$	4-F	CF_2I	60	0.15 (0.002)
10bu	**9v**	$-(CH_2)_2-$	2-(OCF_3)	CF_2Cl	81	>20[a]
10bv	**9v**	$-(CH_2)_2-$	2-(OCF_3)	CF_2Br	40	0.70[a] (0.002)
10bw	**9v**	$-(CH_2)_2-$	2-(OCF_3)	CF_2I	50	1.88 (0.04)

Biological characterization

2-Acylamino-cycloalkylthiophene-3-carboxylic acid arylamides **10aa-10bw** were initially evaluated for inhibition of TMEM16A anion channel function using a cell-based functional plate reader assay as reported.[29, 30, 40] IC_{50} values determined from concentration-inhibition measurements are summarized in Table 3.

The 1st generation library (**10aa-10bj**) showed several compounds with apparent IC_{50} of 0.2-0.3 μM: **10aa** (initial inhibitor), **10ae**, **10ak**, **10au**, **10av**, **10aw**. These results showed that 5-, 6-, and 7-member rings were tolerated at the R^1 position, while compounds based on tetrahydro-4H-pyran-4-one (**10ay-10bc**) were inactive. The best inhibitors contained H, 2- or 4-(CH_3), or 4-F on the aromatic ring (R^2), and CF_3 as the acylamido substituent (R^3). Inhibitors with differing groups at R^2, such as 2-F, 2-Cl, 3-Cl, 4-Cl, 4-(CF_3), 2-(OCF_3), were less potent. Likewise, compounds with alternative substituents at R^3, including CF_2CF_3, CH_3, and CH_2CH_3, also had reduced potency.

Based on results that favored CF_3 at the R^3 position, we designed a 2nd-generation library (**10bk-10bw**) that incorporated novel groups such as chlorodifluoro, bromodifluoro, or difluoroiodo, probing steric and electronic effects at that position. The 2nd-generation library focused on structural features seen in the more active compounds from the 1st-generation library (R^1 = -$(CH_2)_4$-; R^2 = 2-(CH_3), H, or 4-F). One 2nd-generation compound was synthesized that incorporated a heptafluorobutyryl substituent (**10bl**) to evaluate the effect of a multi-carbon fluoroalkyl group. We found three 2nd-generation compounds with lower apparent IC_{50} of 0.08-0.18 μM: **10bk**, **10bm**, and **10bt**. Additionally, the full series of inhibitor candidates (**10aa-10bw**) was subjected to a computational screen for pan-assay interference (PAINS),[42] and all 49 compounds passed.

The most potent TMEM16A inhibitors identified using the semi-quantitative plate reader assay were then studied using a short-circuit current assay in which measured current is a linear measure of TMEM16A Cl^- conductance. Compounds **10aa** (original inhibitor from screen), **10ae**, **10bk**, **10bm**, **10bn** and **10bt** were tested, and compared with reported inhibitors **2**, **3** and **4**. Concentration-dependence for the selected compounds is shown in Figure 3, with IC_{50} values summarized in Table 4. Non-transfected FRT cells shows no signal upon ATP stimulation (Figure S1). By the short-circuit current assay, **10aa** showed an IC_{50} of 0.26 ± 0.10 μM (n=3), similar to the chlorodifluoroacetamide **10bk** with IC_{50} of 0.23 μM. Difluoroiodoacetamides **10bn** and **10bt** were less potent with IC_{50} of 0.73 and 0.60 μM, respectively. Notably, bromodifluoroacetamide **10bm** had IC_{50} of 0.030 ± 0.010 μM (n=3). The IC_{50} of **4** using this assay was 0.11 μM, close to 0.077 μM reported previously;[32] compound **3** had IC_{50} of 1.6 μM by the short-circuit current assay, significantly less potent than the reported IC_{50} of 0.08 μM using a *Xenopus laevis* oocyte assay.[31] Inhibitor **2** was a previously reported to have an IC_{50} of 1 μM.[29]

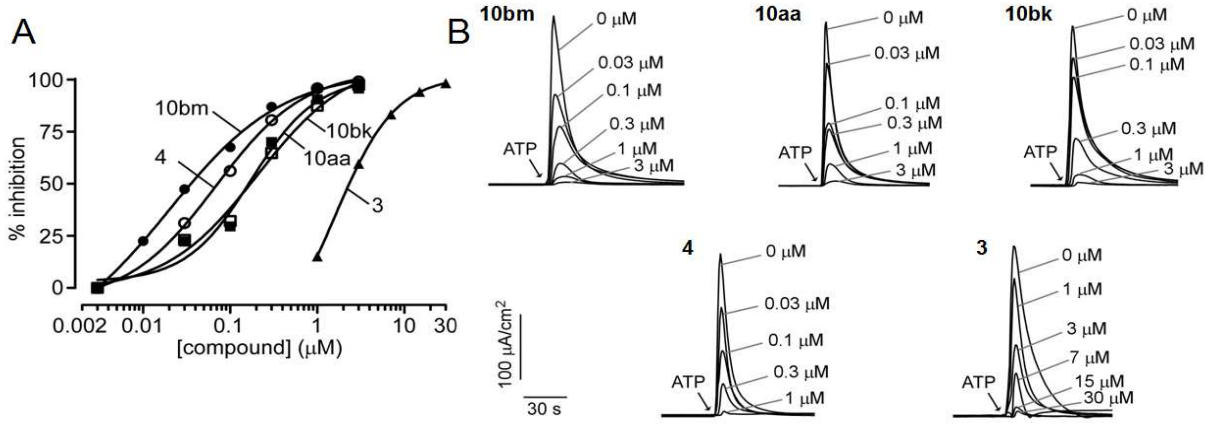

Figure 3. Short-circuit current measurement of TMEM16A inhibition by **10aa**, **10bk** and **10bm**, and previously reported compounds **3** and **4**. Measurements were done in FRT cells expressing human TMEM16A. A. Summary of dose-response data (mean ± SEM, n = 3). B. Examples of original data in which inhibitors were added 5 min prior to TMEM16A activation by 100 μM ATP.

Table 4. Characterization of AACT analogs. Concentration-dependent inhibition of TMEM16A measured by short-circuit current assay; TMEM16B and non-TMEM16 anion conductance measured using a fluorescence plate reader assay; cell viability measured in HT-29 cells. (SEM in parentheses; n=3).

Inhibitor	R^1	R^2	R^3	TMEM16A IC_{50} (μM)	TMEM16B IC_{50} (μM)	HT-29 IC_{50} (μM)	Cellular survival % at 5 μM
2	–	–	–	~1[ref 29]	~4[ref 32]	5.0	97
3	–	–	–	1.6	13	>20	100
4	–	–	–	0.11	>20	0.3	102
10aa	$-(CH_2)_4-$	2-(CH_3)	CF_3	0.26 (0.10)	1.4 (0.05)	4.0	99
10ae	$-(CH_2)_4-$	H	CF_3	0.13	4.6 (0.4)	5.0	97

10bk	$-(CH_2)_4-$	2-(CH_3)	CF_2Cl	0.23	0.4 (0.01)	9.5	98
10bm	$-(CH_2)_4-$	2-(CH_3)	CF_2Br	0.030 (0.010)	0.4 (0.04)	5.4	97
10bn	$-(CH_2)_4-$	2-(CH_3)	CF_2I	0.73	1.4 (0.05)	3.5	96
10bt	$-(CH_2)_4-$	4-F	CF_2I	0.60	1.1 (0.13)	5.0	97

Ion channel specificity and cytotoxicity were determined for the six most potent AACT compounds as well as previously reported compounds **2**, **3** and **4** (Table 4). Selectivity was studied for TMEM16B, an isoform of TMEM16A that functions as a CaCC and regulates action potential firing in olfaction.[43] Inhibition of TMEM16B by the low-potency CaCC inhibitor anthracene-9-carboxylic acid was recently reported.[44] Compounds **3** and **4** (IC_{50} 13 and >20 μM, respectively) were selective against TMEM16B, while **2** was less selective (IC_{50} 4 μM). The AACT compounds displayed modest selectivity against TMEM16B, with an IC_{50} range of 0.4-1.4 μM. Two of the more potent AACT inhibitors of TMEM16A (**10bk** and **10bm**) were also among the more potent against TMEM16B with IC_{50} ~ 0.4 μM. Compound **4** showed 181-fold selectivity against TMEM16B, while **10bm** achieved 13-fold selectivity. We further assayed compound potency on endogenous non-TMEM16A Ca^{2+}-activated Cl^- channel in HT-29 cells.[28] In general, the AACT compounds were weak inhibitors of CaCCs in HT-29 cells (IC_{50} 3.5-9.5 μM), contrasting with **2** (IC_{50} 5 μM), **3** (IC_{50} > 20 μM), and **4** (IC_{50} 0.3 μM). None of the compounds examined showed significant toxicity using an Alamar blue assay at concentrations up to 5 μM. Additionally, none of the compounds inhibited the cAMP-activated Cl^- channel cystic fibrosis transmembrane conductance regulator (CFTR) (data not shown).

Inhibition of TMEM16A by **10bm** was also investigated by the patch-clamp technique using the inside-out configuration. Membrane patches were excised from TMEM16A-expressing FRT cells. With the inside-out configuration, the cytosolic side of the membrane is exposed to the bath solution. To activate TMEM16A, the bath solution contained a free Ca^{2+} concentration of 305 nM. Under

these conditions, relatively large membrane currents were recorded due to the presence of multiple TMEM16A channels (Figure 4). The currents had the typical characteristics of TMEM16A with outward rectification and time-dependent activation at positive membrane potentials. Addition to the bath of **10bm** (250 nM) by perfusion resulted in rapid inhibition of membrane currents, which fully recovered following washout. To further examine the specificity of **10bm**, short-circuit current measurement showed that **10bm** inhibited ionomycin- and carbachol-activated chloride conductance (Figure S2A), indicating that **10bm** did not inhibit chloride conductance through an ATP-stimulated purinergic G protein-coupled receptor mechanism. Further, cytoplasmic calcium was not altered by 1 μM **10bm** as seen in Fluo-4 fluorescence measurement of ATP-stimulated cytoplasmic calcium elevation (Figure S2B). These results support reversible TMEM16A inhibition by **10bm** by a direct interaction mechanism.

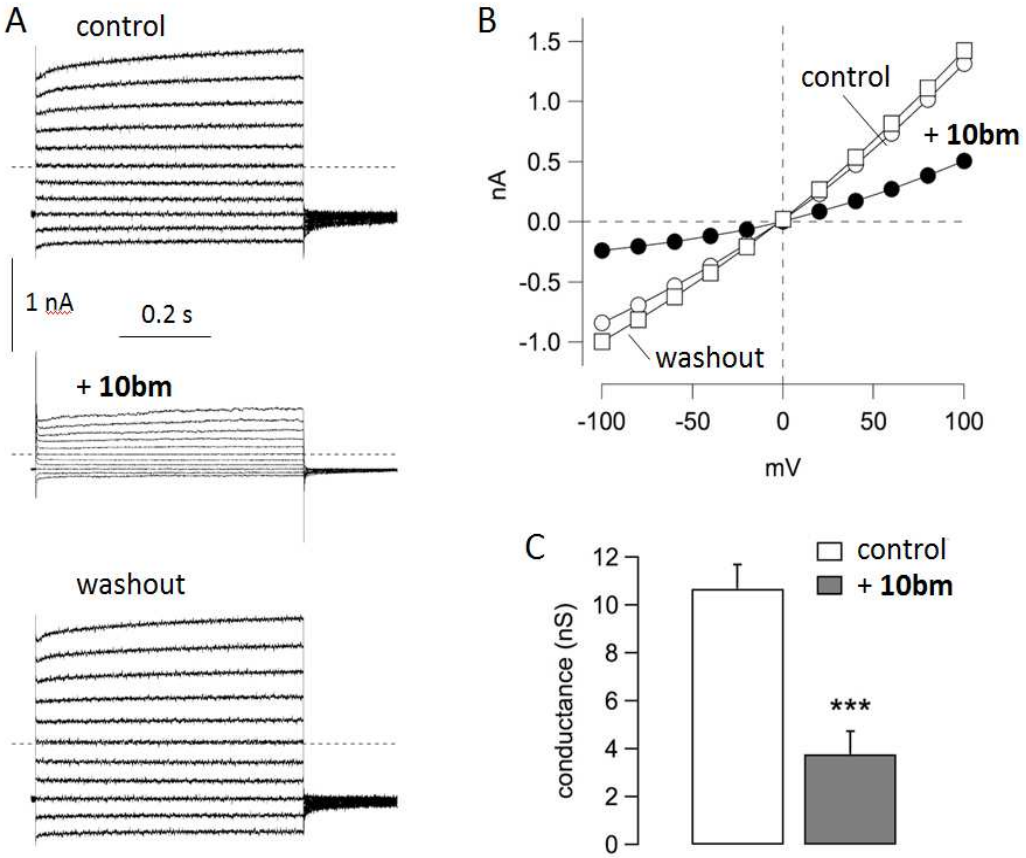

Figure 4. Patch-clamp studies of TMEM16A inhibition by **10bm**. A. Representative currents recorded from an inside-out membrane patch. Cytosolic (bath) free Ca^{2+} concentration was 305 nM. Each panel of traces show superimposed membrane currents elicited at membrane potentials in the range -100 to +100 mV. Currents were recorded under control conditions, after application by perfusion of **10bm** (250 nM), and after washout. B. Current-voltage relationships from the experiment shown in A. Current values were measured at the end of each voltage step. C. Summary of conductance values at +100 mV obtained from five independent experiments (***, $p < 0.001$ by paired t test).

In vitro metabolic stability was determined using a hepatic microsome assay for the most potent AACT inhibitor **10bm** (Figure 5A) and previously reported compound **4**. These compounds were incubated with rat liver microsomes and NADPH, and non-metabolized compounds were quantified by ESI-LCMS. Figure 5B shows near complete degradation of **4** at 180 min, whereas for the same incubation time ~30% of **10bm** remained. Figure 5C summarizes the time course of compound degradation showing remarkably greater stability of **10bm** compared to **4**. Inhibitor **10bm** could be potentially metabolized by amide-bond hydrolysis or oxidation of the benzene or aryl methyl. We speculate that **4** could be oxidized at the aryl methyl or N-N bond; or hydrolyzed at the amide or hydrazone linkages.

We have found the bromodifluoroacetamide functional group present in **10bm** to have long-term shelf stability (> 6 months) as a solid or in DMSO stock solution. In aqueous solution, there was gradual degradation of **10bm**, with 72% and 30% remaining at 1 and 2 days, respectively (Figure S3A). ESI-LCMS analysis suggested that degradation of **10bm** involves: solvolysis, elimination, and hydrolysis of the resulting acid fluoride to a stable N-substituted oxalamic acid (Figure S3B). This solvolytic pathway has not been previously reported for the bromodifluoroacetamide functional group. While we feel this degradation is slow enough to not effect potential pharmacological use of **10bm**, these results discourage multi-day storage in aqueous solution. Kinetic aqueous solubility was measured for **10bm** to be 0.04 mg/mL by titration.

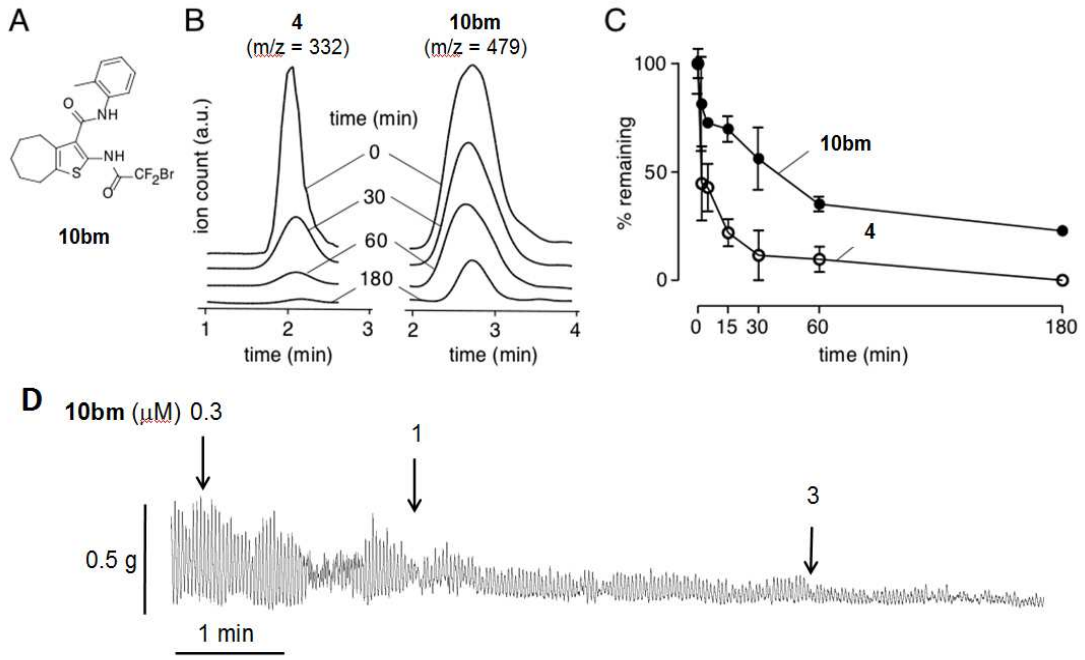

Figure 5. Microsomal stability of **10bm** and **4** in the presence of hepatic microsomes and NADPH, AND inhibition of isometric smooth muscle contractions of *ex vivo* mouse ileum by **10bm**. A. Structure of **10bm**. B. LC/MS traces showing total ion counts as a function of incubation time. C. Summary of in vitro metabolic stability shows percent of remaining compounds over time (mean ± S.E.M., n=3). D. Isometric smooth muscle contraction in mouse ileum showing suppression by **10bm**. Data representative of three separate experiments.

To demonstrate one predicted biological action of TMEM16A inhibition, we measured intestinal smooth muscle contraction. The effect of **10bm** was determined when added to the bath in an *ex vivo* preparation of mouse ileum. As shown in Figure 5D, **10bm** strongly inhibited spontaneous isometric contractions of ileum in a concentration-dependent manner.

CONCLUSION

In conclusion, we identified a new inhibitor of TMEM16A (**10aa**) by screening. The scaffold (designated AACT) is modular, allowing the synthesis and characterization of 48 analogs (**10ab-10bw**). The synthesis utilized substituted aryl cyanoacetamides (**6a-6k**) which were converted to 2-amino-cycloalkylthiophene-3-carboxylic acid arylamides (**9a-9v**) and acylated to afford the final library. The most potent compound in the series (**10bm**) had an IC_{50} of 0.030 μM, making it currently the most potent reported TMEM16A inhibitor. Patch-clamp analysis supported reversible inhibition of TMEM16A by **10bm** by a mechanism involving direct interaction. **10bm** had remarkably greater metabolic stability than the previously reported compound **4**. Finally, **10bm** was shown to inhibit smooth muscle contractions in mouse ileum in concentration-dependent manner, illustrating one of its potential biomedical applications. The high potency and microsomal stability of AACT **10bm** supports its potential as a pharmacological tool to study TMEM16A function and as a potential candidate for further development.

EXPERIMENTAL SECTION

Chemistry

The detailed synthesis of all newly reported synthetic precursor molecules and final inhibitor candidates is presented in Supporting Information. Purity of assayed compounds was >95% based on HPLC-LCMS analysis at 254 nm, and absence of impurities was additionally confirmed by inspection of ^{1}H NMR spectra, and examination of at least one other wavelength (typically 320 nm).

Biology

Cell lines and culture. Fischer Rat Thyroid (FRT) cells stably co-expressing TMEM16A, TMEM16B and human wild-type CFTR and the halide-sensitive yellow fluorescent protein (YFP)-H148Q were cultured as described.[29] HT-29 expressing YFP were cultured as described.[28] FRT cells

were cultured on plastic in Coon's-modified Ham's F12 medium supplemented with 10% fetal bovine serum, 2 mM L-glutamine, 100 units/mL penicillin, and 100 μg/mL streptomycin. For plate reader assays, cells were plated in black 96-well microplates (Corning-Costar Corp., New York, N.Y.) at a density of 20,000 cells per well and assayed 24-48 hours after plating.

TMEM16A functional assay. TMEM16A functional plate-reader assay was done as previously described.[29] Briefly, each well of 96-well plate containing the TMEM16A-expressing FRT cells was washed twice with phosphate buffer saline (PBS) leaving 50 μl. Test compounds (0.5 μl in DMSO) were added to each well at specified concentration. After 10 min each well was assayed individually for TMEM16A-mediated I^- influx by recording fluorescence continuously (400 ms/point) for 2 s (baseline), then 50 μl of 140 mM I^- solution containing 300 μM ATP was added at 2 s, and fluorescence was further read for 12 s. The initial rate of I- influx following each of the solution additions was computed from fluorescence data by nonlinear regression. TMEM16B activity was assayed similarly as described[29] using FRT cells co-expressing YFP and TMEM16B.

***In silico* PAINS assay.** A computational screen for pan-assay interference compounds (PAINS)[42] was employed to identify substructures associated with promiscuous inhibition. The full series of inhibitor candidates (**10aa-10bw**) was converted to SMILES strings, and submitted to an internet-based implementation of the PAINS filter (http://cbligand.org/PAINS), maintained by Prof. Xiang-Qun (Sean) Xie's laboratory at University of Pittsburgh School of Pharmacy.

Short-circuit current measurement. Short-circuit current measurements were done as described.[30] Briefly, Snapwell inserts (Corning Costar, Corning, NY) containing TMEM16A-expressing FRT cells were mounted in Ussing chambers (Physiological Instruments, San Diego, CA). The hemichambers were filled with 5 ml of HCO_3^- buffered solution (basolateral) and half-Cl^- solution (apical), and the basolateral membrane was permeabilized with 250 μg/ml amphotericin B. Solutions were bubbled with 95% O_2/5% CO_2 and maintained at 37°C, and short-circuit current was

measured on a DVC-1000 voltage clamp (World Precision Instruments Inc., Sarasota, FL) using Ag/AgCl electrodes and 3 M KCl agar bridges.

Patch clamp. Currents were recorded from inside-out membrane patches excised from FRT cells stably expressing TMEM16A. The pipette (extracellular) solution contained (in mM): 150 NaCl, 1 $CaCl_2$, 1 $MgCl_2$, 10 glucose, 10 mannitol, 10 Na-Hepes (pH 7.3). The bath (intracellular) solution contained (in mM): 130 CsCl, 1 $MgCl_2$, 10 EGTA, 10 Na-Hepes (pH 7.3), and 8 $CaCl_2$ to obtain the desired free Ca^{2+} concentration of 305 nM. The electrical resistance of micropipettes was 3-7 MΩ. The protocol for stimulation consisted of 600 ms voltage steps in the range from -100 to +100 mV (with 20 mV increments) starting from a holding potential of -60 mV. The interval between steps was 4 s. Membrane currents were filtered at 1 kHz and digitized at 5 kHz. Data were analyzed using the Igor software (Wavemetrics, Portland, OR) with custom software kindly provided by Dr. Oscar Moran.

In vitro metabolic stability. Compounds (each 10 uM) were incubated for specific time points (2, 5, 15, 30, 60, 180 min) with shaking at 37 °C with rat liver microsomes (1 mg protein/mL, Sigma-Aldrich, St. Louis, MO) in potassium phosphate buffer (100 mM) containing 1 mM NADPH. The mixture was then chilled on ice, and 0.5 mL of ice-cold ethyl acetate was added. Samples were centrifuged for 15 min at 3000 RPM. The supernatant was evaporated to dryness, and the residue was dissolved in 80 μL of mobile phase (acetonitrile:/water, 3:1, containing 0.1% formic acid) for LC/MS. Reverse-phase HPLC separation was carried out using a Waters C_{18} column (2.1 mm × 100 mm, 3.5 mm particle size) equipped with a solvent delivery system (Waters model 2690, Milford, MA). The solvent system consisted of a linear gradient from 5% to 95% acetonitrile run over 16 min (0.2 mL/min flow rate).

Plate reader assays of chloride channel function. CFTR inhibition was assayed as described.[45] Briefly, FRT cells co-expressing YFP and wildtype CFTR were washed with phosphate-buffered saline (PBS) and then incubated for 15 min with test compounds in PBS containing 20 μM forskolin.

I^- influx was measured in a plate reader with initial baseline read for 2 s and then for 12 s after rapid addition of an I^- containing solution. Activity of non-TMEM16A CaCC was assayed as described[28] in HT-29 cells expressing YFP. In each assay initial rates of I− influx were computed as a linear measure of channel function.

Cytotoxicity. FRT cells were cultured overnight in black 96-well Costar microplates and incubated with 5 μM test compounds for 8 h. Cytotoxicity was measured by Alamar Blue assay (Invitrogen, Carlsbad, CA) as per the manufacturer's instructions.

Ex vivo intestinal contractility. Adult mice (CD1 genetic background) were euthanized by avertin overdose (200 mg/kg, 2,2,2-tribromethanol, Sigma-Aldrich) and ileal segments of ~2 cm length were isolated and washed with Krebs-Henseleit buffer (pH 7.4, in mM: 118 NaCl, 4.7 KCl, 1.2 $MgSO_4$, 1.2 KH_2PO_4, 25 $NaHCO_3$, 2.5 $CaCl_2$, 11 D-glucose). The ends of the ileal segments were tied, connected to a force transducer (Biopac Systems, Goleta, CA) and tissues were transferred to an organ chamber (Biopac Systems) containing Krebs-Henseleit buffer at 37°C aerated with 95% O_2, 5% CO_2. Tissues were stabilized for 60 min with resting tension of 0.5 g and solutions were changed every 15 min. Effects of **10bm** on baseline isometric intestinal contractions were recorded. Animal protocols were approved by the UCSF Institutional Animal Care and Use Committee (approval number: AN108711-02A) and were conducted according with the NIH guidelines for the care and use of animals.

Aqueous stability. Duplicate HPLC samples were prepared in H_2O (20% DMSO) containing **10bm** (100 μM) and aqueous stable internal standard 5-chloro-3-phenyl-2,1-benzisoxazole (100 μM). The samples were incubated at 25 ^oC for 3 days, and analyzed daily by ESI-LCMS showing gradual decomposition to the corresponding oxalamic acid.

Aqueous kinetic solubility. To a series of 2 mL aliquots of PBS solution were added increasing quantities of **10bm** (30 mM DMSO stock solution). The titration point was determined at 6.5 μL of added stock solution, corresponding to 0.04 mg/ml kinetic solubility.

AUTHOR INFORMATION

Corresponding Author. *Phone: 415-338-6495. Fax: 415-405-0377. E-mail: marc@sfsu.edu.

Notes. Drs. Anderson, Phuan and Verkman are named co-inventors on a provisional patent filing with rights owned by UCSF and SFSU.

ACKNOWLEDGEMENTS

This study was supported by NIH grants R15 GM102874, P30 DK072517, R01 DK099803, R01 DK075302, R01 DK101373, and R01 EY13574, and a grant from the Cystic Fibrosis Foundation. Patch-clamp studies were supported by grants from Ministero della Salute (Ricerca Corrente: Cinque per mille) and Telethon Foundation to LJVG (TMLGCBX16TT). The authors acknowledge Dr. Robert Yen at the SFSU Mass Spectrometry Facility and Dr. Mark Swanson at SFSU NMR Facility.

ABBREVIATIONS USED

AACT, 2-acylamino-cycloalkylthiophene-3-carboxylic acid arylamide; ANO1, anoctamin 1; CaCC, calcium-activated chloride channel; CFTR, cystic fibrosis transmembrane regulator; DCM, dichloromethane; 4-DMAP, N,N-dimethylaminopyridine; DMF, N,N-dimethylformamide; DMSO, dimethyl sulfoxide; EDCI-HCl, 1-(3-dimethylaminopropyl)-3-ethylcarbodiimide hydrochloride; FPR, fluorescent plate reader; FRT, Fischer Rat Thyroid; PAINS, pan assay interference compounds; PBS, phosphate-buffered saline; RT, room temperature; TLC, thin layer chromatography; TMEM16A, transmembrane protein 16A; YFP, yellow fluorescent protein.

ASSOCIATED CONTENT

Supporting Information Available. Supporting Information is available free of charge on the ACS Publications Website at DOI: xxxxxxxxx/yyyyyyyyy:

Control measurement of short-circuit current in non-transfected cells; time-course and proposed mechanism of aqueous degradation of inhibitor **10bm**; synthesis details and spectroscopic characterization of new molecules (PDF).

Molecular strings for all final inhibitor candidates (CSV).

REFERENCES

1. Pedemonte, N.; Galietta, L. J. Structure and function of TMEM16 proteins (anoctamins). *Physiol. Rev.* **2014,** *94*, 419-459.

2. Picollo, A.; Malvezzi, M.; Accardi, A. TMEM16 proteins: unknown structure and confusing functions. *J. Mol. Bio.* **2015,** *427*, 94-105.

3. Oh, U.; Jung, J. Cellular functions of TMEM16/anoctamin. *Pfluegers Arch.* **2016,** *468*, 443-453.

4. Qu, Z.; Yao, W.; Yao, R.; Liu, X.; Yu, K.; Hartzell, C. The Ca^{2+} -activated Cl^{-} channel, ANO1 (TMEM16A), is a double-edged sword in cell proliferation and tumorigenesis. *Cancer Med.* **2014,** *3*, 453-461.

5. Wanitchakool, P.; Wolf, L.; Koehl, G. E.; Sirianant, L.; Schreiber, R.; Kulkarni, S.; Duvvuri, U.; Kunzelmann, K. Role of anoctamins in cancer and apoptosis. *Philos. Trans. R. Soc., B* **2014,** *369*, 20130096.

6. Guan, L.; Song, Y.; Gao, J.; Gao, J.; Wang, K. Inhibition of calcium-activated chloride channel ANO1 suppresses proliferation and induces apoptosis of epithelium originated cancer cells. *Oncotarget* **2016,** *7*, 78619-78630.

7. Li, Q.; Zhi, X.; Zhou, J.; Tao, R.; Zhang, J.; Chen, P.; Roe, O. D.; Sun, L.; Ma, L. Circulating tumor cells as a prognostic and predictive marker in gastrointestinal stromal tumors: a prospective study. *Oncotarget* **2016,** *7*, 36645–36654.

8. Shang, L.; Hao, J. J.; Zhao, X. K.; He, J. Z.; Shi, Z. Z.; Liu, H. J.; Wu, L. F.; Jiang, Y. Y.; Shi, F.; Yang, H.; Zhang, Y.; Liu, Y. Z.; Zhang, T. T.; Xu, X.; Cai, Y.; Jia, X. M.; Li, M.; Zhan, Q. M.; Li, E. M.; Wang, L. D.; Wei, W. Q.; Wang, M. R. ANO1 protein as a potential biomarker for esophageal cancer prognosis and precancerous lesion development prediction. *Oncotarget* **2016,** *7*, 24374-24382.

9. Wu, H.; Guan, S.; Sun, M.; Yu, Z.; Zhao, L.; He, M.; Zhao, H.; Yao, W.; Wang, E.; Jin, F.; Xiao, Q.; Wei, M. Ano1/TMEM16A Overexpression is associated with good prognosis in PR-positive or HER2-negative breast cancer patients following tamoxifen treatment. *PLoS One* **2015,** *10*, e0126128.

10. Caputo, A.; Caci, E.; Ferrera, L.; Pedemonte, N.; Barsanti, C.; Sondo, E.; Pfeffer, U.; Ravazzolo, R.; Zegarra-Moran, O.; Galietta, L. J. TMEM16A, a membrane protein associated with calcium-dependent chloride channel activity. *Science* **2008,** *322*, 590-594.

11. Yang, Y. D.; Cho, H.; Koo, J. Y.; Tak, M. H.; Cho, Y.; Shim, W. S.; Park, S. P.; Lee, J.; Lee, B.; Kim, B. M.; Raouf, R.; Shin, Y. K.; Oh, U. TMEM16A confers receptor-activated calcium-dependent chloride conductance. *Nature* **2008,** *455*, 1210-1215.

12. Schroeder, B. C.; Cheng, T.; Jan, Y. N.; Jan, L. Y. Expression cloning of TMEM16A as a calcium-activated chloride channel subunit. *Cell* **2008,** *134*, 1019-1029.

13. Ferrera, L.; Caputo, A.; Ubby, I.; Bussani, E.; Zegarra-Moran, O.; Ravazzolo, R.; Pagani, F.; Galietta, L. J. Regulation of TMEM16A chloride channel properties by alternative splicing. *J. Biol. Chem.* **2009,** *284*, 33360-33368.

14. Tian, Y.; Kongsuphol, P.; Hug, M.; Ousingsawat, J.; Witzgall, R.; Schreiber, R.; Kunzelmann, K. Calmodulin-dependent activation of the epithelial calcium-dependent chloride channel TMEM16A. *FASEB J.* **2011,** *25*, 1058-1068.

15. Tian, Y.; Schreiber, R.; Kunzelmann, K. Anoctamins are a family of Ca^{2+}-activated Cl- channels. *J. Cell. Sci.* **2012,** *125*, 4991-4998.

16. Sung, T. S.; O'Driscoll, K.; Zheng, H.; Yapp, N. J.; Leblanc, N.; Koh, S. D.; Sanders, K. M. Influence of intracellular Ca^{2+} and alternative splicing on the pharmacological profile of ANO1 channels. *Am. J. Physiol. Cell Physiol.* **2016,** *311*, C437-451.

17. Yu, K.; Duran, C.; Qu, Z.; Cui, Y. Y.; Hartzell, H. C. Explaining calcium-dependent gating of anoctamin-1 chloride channels requires a revised topology. *Circ. Res.* **2012,** *110*, 990-999.

18. Tien, J.; Peters, C. J.; Wong, X. M.; Cheng, T.; Jan, Y. N.; Jan, L. Y.; Yang, H. A comprehensive search for calcium binding sites critical for TMEM16A calcium-activated chloride channel activity. *Elife* **2014,** *3*, e02772.

19. Yuan, H.; Gao, C.; Chen, Y.; Jia, M.; Geng, J.; Zhang, H.; Zhan, Y.; Boland, L. M.; An, H. Divalent cations modulate TMEM16A calcium-activated chloride channels by a common mechanism. *J. Membr. Biol.* **2013,** *246*, 893-902.

20. Peters, C. J.; Yu, H.; Tien, J.; Jan, Y. N.; Li, M.; Jan, L. Y. Four basic residues critical for the ion selectivity and pore blocker sensitivity of TMEM16A calcium-activated chloride channels. *Proc. Natl. Acad. Sci. U. S. A.* **2015,** *112*, 3547-3552.

21. Cruz-Rangel, S.; De Jesus-Perez, J. J.; Contreras-Vite, J. A.; Perez-Cornejo, P.; Hartzell, H. C.; Arreola, J. Gating modes of calcium-activated chloride channels TMEM16A and TMEM16B. *J. Physiol.* **2015,** *593*, 5283-5298.

22. Fallah, G.; Romer, T.; Detro-Dassen, S.; Braam, U.; Markwardt, F.; Schmalzing, G. TMEM16A(a)/anoctamin-1 shares a homodimeric architecture with CLC chloride channels. *Mol. Cell. Proteomics* **2011,** *10*, M110 004697.

23. Sheridan, J. T.; Worthington, E. N.; Yu, K.; Gabriel, S. E.; Hartzell, H. C.; Tarran, R. Characterization of the oligomeric structure of the Ca^{2+}-activated Cl^- channel Ano1/TMEM16A. *J. Biol. Chem.* **2011,** *286*, 1381-1388.

24. Tien, J.; Lee, H. Y.; Minor, D. L., Jr.; Jan, Y. N.; Jan, L. Y. Identification of a dimerization domain in the TMEM16A calcium-activated chloride channel (CaCC). *Proc. Natl. Acad. Sci. U. S. A.* **2013,** *110*, 6352-6357.

25. Scudieri, P.; Musante, I.; Gianotti, A.; Moran, O.; Galietta, L. J. Intermolecular interactions in the TMEM16A dimer controlling channel activity. *Sci. Rep.* **2016,** *6*, 38788.

26. Brunner, J. D.; Lim, N. K.; Schenck, S.; Duerst, A.; Dutzler, R. X-ray structure of a calcium-activated TMEM16 lipid scramblase. *Nature* **2014,** *516*, 207-212.

27. Jia, L.; Liu, W.; Guan, L.; Lu, M.; Wang, K. Inhibition of calcium-activated chloride channel ANO1/TMEM16A suppresses tumor growth and invasion in human lung cancer. *PLoS One* **2015,** *10*, e0136584.

28. De La Fuente, R.; Namkung, W.; Mills, A.; Verkman, A. S. Small-molecule screen identifies inhibitors of a human intestinal calcium-activated chloride channel. *Mol. Pharmacol.* **2008,** *73*, 758-768.

29. Namkung, W.; Phuan, P. W.; Verkman, A. S. TMEM16A inhibitors reveal TMEM16A as a minor component of calcium-activated chloride channel conductance in airway and intestinal epithelial cells. *J. Biol. Chem.* **2011,** *286*, 2365-2374.

30. Piechowicz, K. A.; Truong, E. C.; Javed, K. M.; Chaney, R. R.; Wu, J. Y.; Phuan, P. W.; Verkman, A. S.; Anderson, M. O. Synthesis and evaluation of 5,6-disubstituted thiopyrimidine aryl aminothiazoles as inhibitors of the calcium-activated chloride channel TMEM16A/Ano1. *J. Enzyme Inhib. Med. Chem.* **2016**, *31*, 1362-1368.

31. Oh, S. J.; Hwang, S. J.; Jung, J.; Yu, K.; Kim, J.; Choi, J. Y.; Hartzell, H. C.; Roh, E. J.; Lee, C. J. MONNA, a potent and selective blocker for transmembrane protein with unknown function 16/anoctamin-1. *Mol. Pharmacol.* **2013,** *84*, 726-735.

32. Seo, Y.; Lee, H. K.; Park, J.; Jeon, D. K.; Jo, S.; Jo, M.; Namkung, W. Ani9, A novel potent small-molecule ANO1 inhibitor with negligible effect on ANO2. *PLoS One* **2016,** *11*, e0155771.

33. Davis, A. J.; Shi, J.; Pritchard, H. A.; Chadha, P. S.; Leblanc, N.; Vasilikostas, G.; Yao, Z.; Verkman, A. S.; Albert, A. P.; Greenwood, I. A. Potent vasorelaxant activity of the TMEM16A inhibitor $T16A_{inh}$ -A01. *Br. J. Pharmacol.* **2013,** *168*, 773-784.

34. Sun, H.; Xia, Y.; Paudel, O.; Yang, X. R.; Sham, J. S. Chronic hypoxia-induced upregulation of Ca^{2+}-activated Cl- channel in pulmonary arterial myocytes: a mechanism contributing to enhanced vasoreactivity. *J. Physiol.* **2012,** *590*, 3507-3521.

35. Mroz, M. S.; Keely, S. J. Epidermal growth factor chronically upregulates Ca^{2+}-dependent Cl^- conductance and TMEM16A expression in intestinal epithelial cells. *J. Physiol.* **2012,** *590*, 1907-1920.

36. Li, R. S.; Wang, Y.; Chen, H. S.; Jiang, F. Y.; Tu, Q.; Li, W. J.; Yin, R. X. TMEM16A contributes to angiotensin II-induced cerebral vasoconstriction via the RhoA/ROCK signaling pathway. *Mol. Med. Rep.* **2016,** *13*, 3691-3699.

37. Bill, A.; Hall, M. L.; Borawski, J.; Hodgson, C.; Jenkins, J.; Piechon, P.; Popa, O.; Rothwell, C.; Tranter, P.; Tria, S.; Wagner, T.; Whitehead, L.; Gaither, L. A. Small molecule-facilitated degradation of ANO1 protein: a new targeting approach for anticancer therapeutics. *J. Biol. Chem.* **2014,** *289*, 11029-11041.

38. Boedtkjer, D. M.; Kim, S.; Jensen, A. B.; Matchkov, V. M.; Andersson, K. E. New selective inhibitors of calcium-activated chloride channels - $T16A_{inh}A01$, $CaCC_{inh}A01$ and MONNA - what do they inhibit? *Br. J. Pharmacol.* **2015,** *172*, 4158-4172.

39. Liu, Y.; Zhang, H.; Huang, D.; Qi, J.; Xu, J.; Gao, H.; Du, X.; Gamper, N. Characterization of the effects of Cl^- channel modulators on TMEM16A and bestrophin-1 Ca^{2+} activated Cl^- channels. *Pfluegers Arch.* **2015,** *467*, 1417-1430.

40. Namkung, W.; Yao, Z.; Finkbeiner, W. E.; Verkman, A. S. Small-molecule activators of TMEM16A, a calcium-activated chloride channel, stimulate epithelial chloride secretion and intestinal contraction. *FASEB J.* **2011,** *25*, 4048-4062.

41. Oh, S.; Kwon, B.; Kong, S.; Yang, G.; Lee, N.; Han, D.; Goo, J.; Siqueira-Neto, J. L.; Freitas-Junior, L. H.; Liuzzi, M.; Lee, J.; Song, R. Synthesis and biological evaluation of 2-acetamidothiophene-3-carboxamide derivatives against Leishmania donovani. *MedChemComm* **2014,** *5*, 142-146.

42. Baell, J. B.; Holloway, G. A. New substructure filters for removal of pan assay interference compounds (PAINS) from screening libraries and for their exclusion in bioassays. *J. Med. Chem.* **2010,** *53*, 2719-2740.

43. Pietra, G.; Dibattista, M.; Menini, A.; Reisert, J.; Boccaccio, A. The Ca^{2+}-activated Cl^{-} channel TMEM16B regulates action potential firing and axonal targeting in olfactory sensory neurons. *J. Gen. Physiol* **2016,** *148*, 293-311.

44. Cherian, O. L.; Menini, A.; Boccaccio, A. Multiple effects of anthracene-9-carboxylic acid on the TMEM16B/anoctamin2 calcium-activated chloride channel. *Biochim. Biophys. Acta* **2015,** *1848*, 1005-1013.

45. Tradtrantip, L.; Sonawane, N. D.; Namkung, W.; Verkman, A. S. Nanomolar potency pyrimido-pyrrolo-quinoxalinedione CFTR inhibitor reduces cyst size in a polycystic kidney disease model. *J. Med. Chem.* **2009,** *52*, 6447-6455.

TABLE OF CONTENTS FIGURE

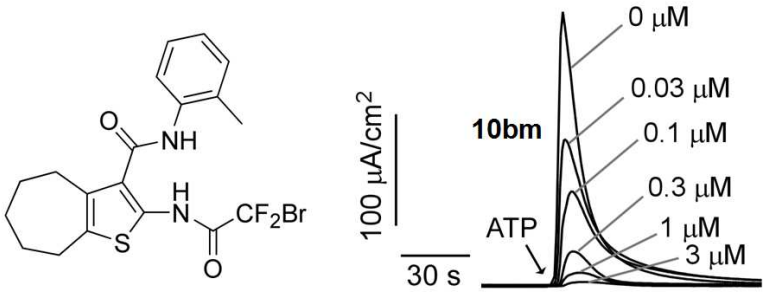

10bm IC_{50} = 30 nM TMEM16A short-circuit current